Supporting Information

to

Sunlight can convert atmospheric aerosols into a glassy solid state and modify their environmental impacts

Vahe J. Baboomian[1*], Giuseppe V. Crescenzo[2*], Yuanzhou Huang[2], Fabian Mahrt[2,3], Manabu Shiraiwa[1], Allan K. Bertram[2], and Sergey A. Nizkorodov[1]

[1]Department of Chemistry, University of California, Irvine, Irvine, CA 92697, USA

[2]Department of Chemistry, University of British Columbia, Vancouver, BC, Canada

[3]Laboratory of Environmental Chemistry, Paul Scherrer Institute, 5232 Villigen, Switzerland

Corresponding authors: Allan K. Bertram, bertram@chem.ubc.ca, and Sergey A. Nizkorodov, nizkorod@uci.edu.

*These authors contributed equally to this work

Table of Contents

Section S1: Poke-Flow Measurements

Table S1: Summary of SOA production conditions in both the environmental chamber and aerosol flow tube. In the case of SOA generated in the flow tube, SOA samples for viscosity measurements and HRMS analysis were collected consecutively on the same day.

VOC Precursor	Production Method	VOC concentration / ppm	Ozone concentration / ppm	SOA mass concentration / μg m^{-3}	Aged or Control	Use
d-limonene	Environmental chamber	0.20	7.4	396	Aged	Viscosity measurements
d-limonene	Environmental chamber	0.20	6.5	286	Control	Viscosity measurements
d-limonene	Environmental chamber	0.20	7.0	604	Aged	HRMS analysis
d-limonene	Environmental chamber	0.20	6.0	530	Control	HRMS analysis
d-limonene	Flow tube	11	7.5	1700	Aged/Control	Viscosity measurements & HRMS analysis
α-pinene	Flow tube	11	7.0	1700	Aged/Control	Viscosity measurements & HRMS analysis

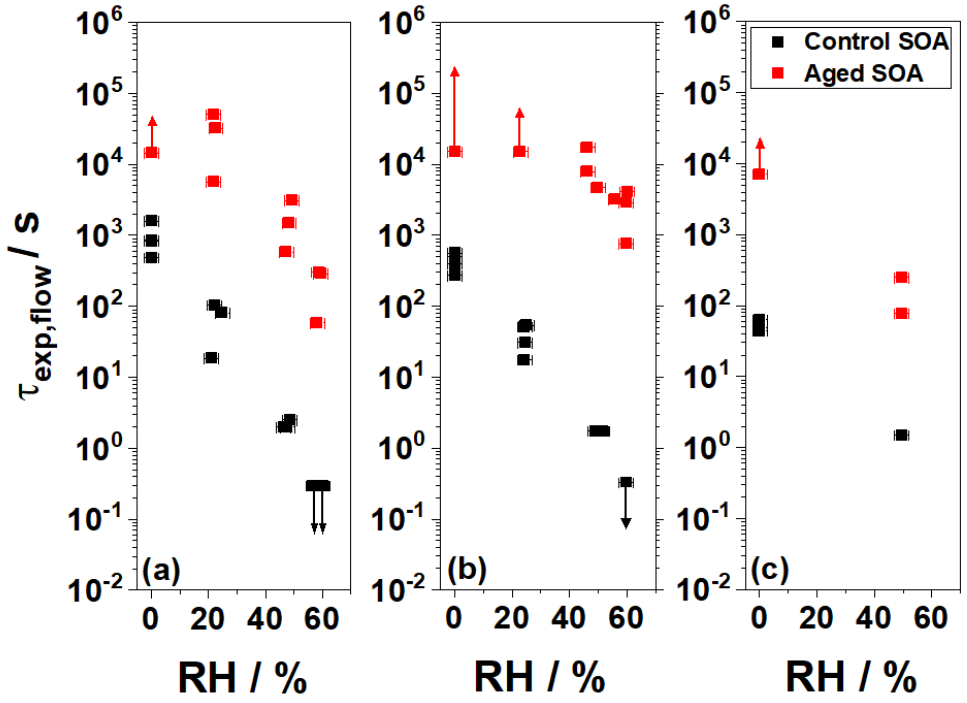

Figure S1: Summary of the experimental flow times ($\tau_{exp,flow}$) as a function of relative humidity (RH) obtained from room temperature (292 K) poke-flow experiments. Black squares correspond to control SOA, red squares correspond to aged SOA. Panel (a) corresponds to d-limonene SOA produced in an environmental chamber, panel (b) corresponds to d-limonene SOA prepared in the flow tube and panel (c) represents α-pinene prepared in the flow tube.

COMSOL Simulation Parameters

Table S2: COMSOL parameters used to simulate the experimentally observed flow times and determine the upper and lower bounds of viscosities of the SOA particles.

SOA type	Surface tension / mN m^{-1}	Slip length / m	Contact angle / °
d-limonene Control	25.9[a]–45[b]	5×10^{-9}–1×10^{-6} [c]	50.4–83.7[d]
d-limonene Aged	25.9[a]–45[b]	5×10^{-9}–1×10^{-6} [c]	55.5–65.0[d]
α-pinene Control and Aged	25.3[a]–45[b]	5×10^{-9}–1×10^{-6} [c]	52.7–67.7[d]

[a] As a conservative lower limit to the surface tension of the d-limonene and α-pinene SOA, the surface tension of the pure liquids were used. Surface tensions were determined with the ACD/Labs Percepta Platform-PhysChem Module, retrieved from ChemSpider January 14, 2022.

[b] This upper limit is consistent with surface tension measurements of SOA at RH $\lesssim$ 65% RH and surface tensions reported for alcohols, organic acids, esters, and ketones, as well as surface tension measurements of water solutions containing SOA products[1–4].

[c] Range based on measurements of the slip length of organic compounds and water on hydrophobic surfaces[5–17].

[d] Contact angles determined by measuring the height and radii of individual droplets using a confocal microscope following the method of Chesna et al.[18]. Note: the simulated viscosities depend only weakly on the contact angle. Changing the contact angle by ±10% changes the simulated viscosity on average by ±15%, which is small compared to the overall uncertainties associated with the simulated viscosities.

The Effect of Evaporation on Particle Size and Viscosity

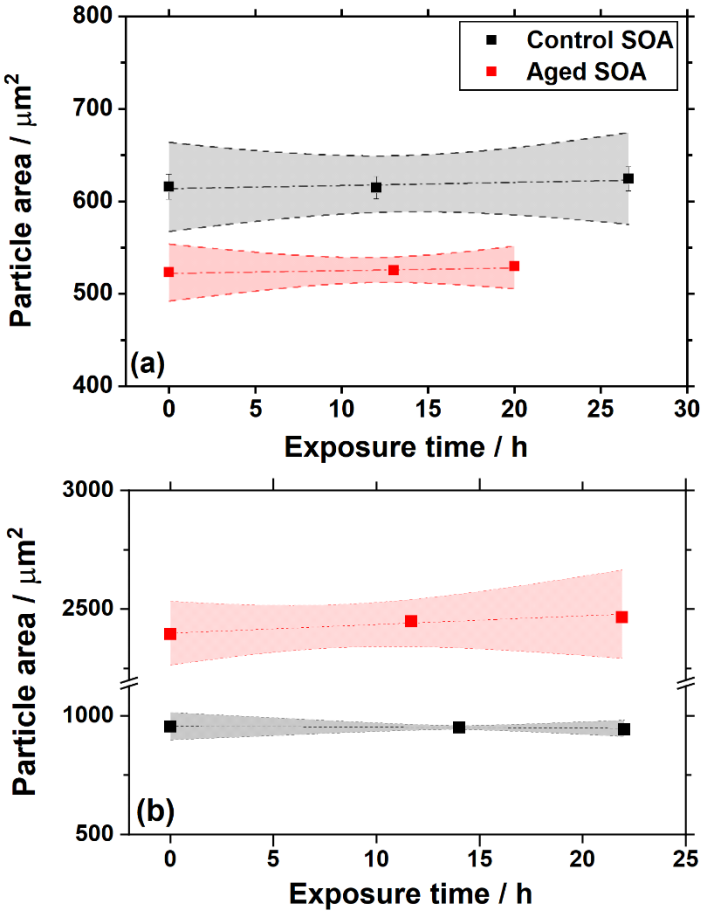

Figure S2: Particle evaporation tests in the flow cell used for poke-flow experiments. To check for possible evaporation of the particles during poke-flow experiments, the particle area was monitored over the course of 24 h for d-limonene aged and control SOA. Panel (a) represents exposure times under dry conditions (≈ 0% RH) in the poking chamber, and panel (b) represents exposure times under 60% RH. The confidence bands represent the standard deviation of repeated particle area measurements of a single particle at a given time. SOA was produced by ozonolysis in an environmental chamber.

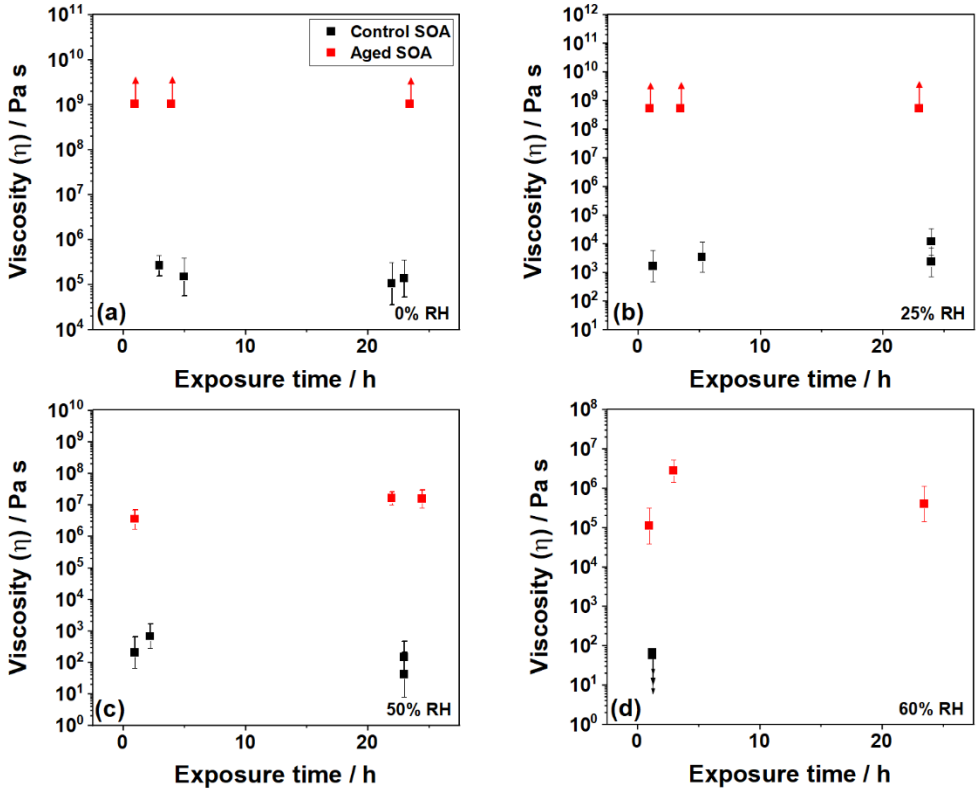

Figure S3: Dependence of viscosity on the time particles spent in the poke-flow cell before the measurement. To ensure that particles were at equilibrium at a given RH, viscosities of d-limonene aged and control SOA were obtained as a function of exposure time at different RH levels. Panels correspond to (a) 0% RH, (b) 25% RH, (c) 50% RH, and (d) 60% RH in the poking chamber. Viscosities are identical within uncertainties after conditioning for 1–24 h. SOA was produced by ozonolysis in an environmental chamber.

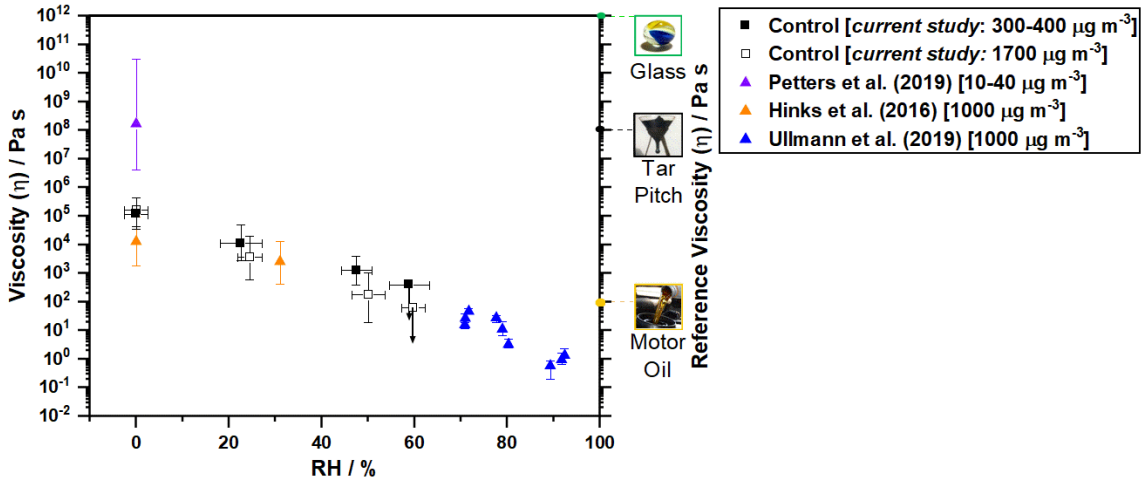

Figure S4: Comparison of published viscosities of limonene SOA to our control d-limonene SOA produced in an environmental chamber and flow tube. Mass concentrations used in the production of SOA are listed for comparison[19–21]. Error bars from Petters et al. correspond to the uncertainty in the temperature extrapolated glass transition temperature of ± 10 K[19].

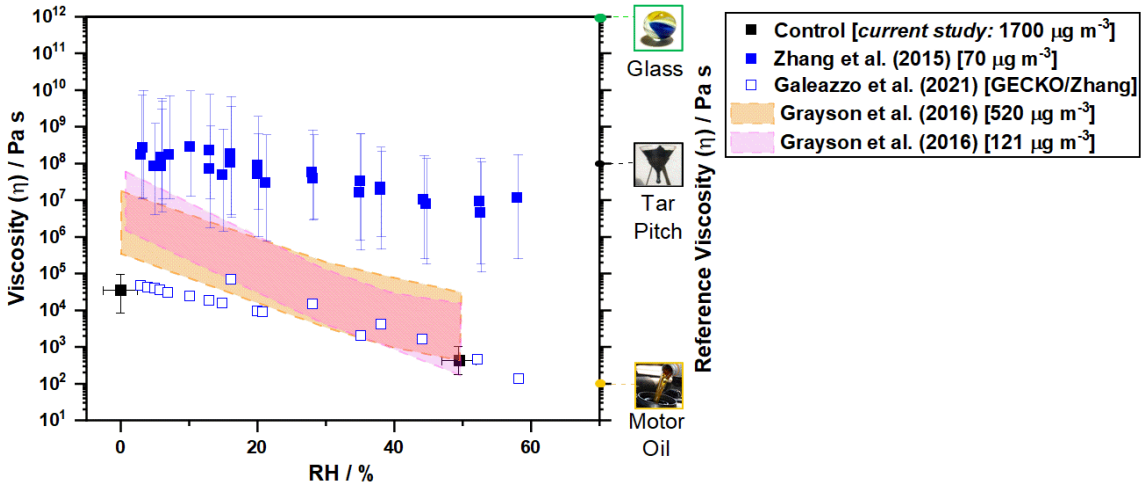

Figure S5: Comparison of published viscosities of α-pinene SOA to our control α-pinene SOA. Mass concentrations used in the production of SOA are listed for comparison of viscosities[22–24]. For Galeazzo et al. (2021)[23], explicit modelling of gas-phase oxidation was performed using GECKO-A model.

Section S2: High-Resolution Mass Spectrometry (HRMS) Average Characteristics and Prediction of SOA Viscosity Using HRMS Data

Table S3: Summary of chemical composition characteristics of d-limonene ozonolysis SOA produced in an environmental chamber and a flow tube, and of α-pinene ozonolysis SOA produced in a flow tube. Dimer-to-monomer ratio is the ratio of combined peak abundances above 300 Da to that below 300 Da. This threshold was chosen as the center between the modes of the monomer (peaking around 200 Da) and dimer (peaking around 400 Da) compounds. All averages are weighted by the normalized peak abundance in the mass spectra. Both $T_{g,org}$ and $T_{g,org,uncorr}$ are included in the table to show the glass transition temperature with and without any corrections for the higher ionization efficiency of higher molecular weight compounds in the HRMS measurements.

	Dimer: Monomer Ratio	Avg. MW / g mol^{-1}	Avg. O:C	Avg. H:C	Avg. DBE	Avg. #C	$T_{g,org}$ / K	$T_{g,org,uncorr}$ / K
Control Chamber d-limonene SOA	0.332	245.6	0.54	1.52	4.14	11.24	273.1	287.1
Aged Chamber d-limonene SOA	0.463	270.3	0.61	1.44	4.92	11.89	283.3	297.6
Difference (aged – control)	↑ 0.130 (39.2%)	↑ 24.7 (10.0%)	↑ 0.07 (12.2%)	↓ 0.08 (5.4%)	↑ 0.77 (18.7%)	↑ 0.65 (5.8%)	↑ 10.2 (3.7%)	↑ 10.5 (3.7%)
Control Flow Tube d-limonene SOA	0.625	281.0	0.47	1.52	4.14	13.39	273.3	294.3
Aged Flow Tube d-limonene SOA	0.871	313.9	0.55	1.42	5.21	14.22	287.0	307.4
Difference (aged – control)	↑ 0.246 (39.4%)	↑ 32.9 (11.7%)	↑ 0.08 (17.0%)	↓ 0.10 (6.6%)	↑ 1.07 (25.8%)	↑ 0.83 (6.2%)	↑ 13.7 (5.0%)	↑ 13.1 (4.4%)
Control Flow Tube α-pinene SOA	0.600	265.0	0.46	1.45	3.91	12.94	273.3	290.6
Aged Flow Tube α-pinene SOA	0.765	290.1	0.51	1.39	4.63	13.56	283.1	300.5
Difference (aged – control)	↑ 0.165 (27.5%)	↑ 25.1 (9.5%)	↑ 0.05 (10.9%)	↓ 0.06 (4.1%)	↑ 0.72 (18.4%)	↑ 0.62 (4.8%)	↑ 9.8 (3.6%)	↑ 10 (3.4%)

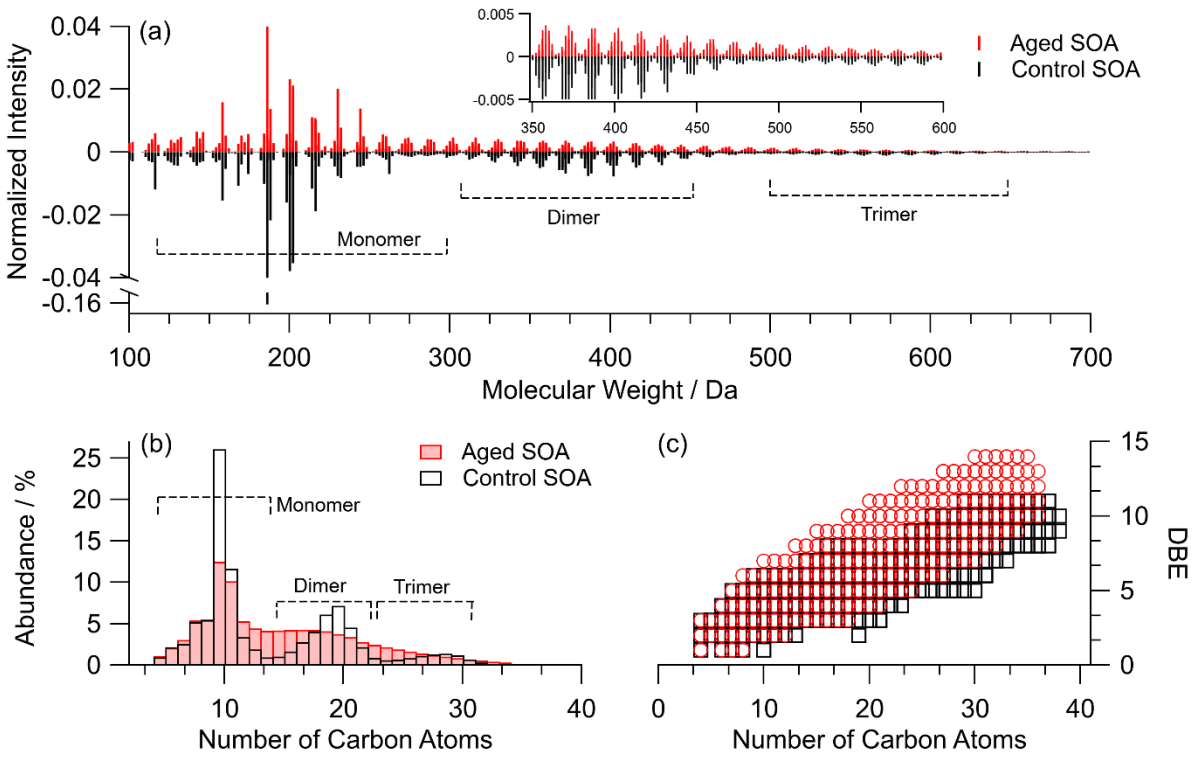

Figure S6: High resolution mass spectrometry (HRMS) analysis of d-limonene ozonolysis SOA produced in the flow tube and changes in chemical composition due to aging. Panel (a) shows mass spectra of the aged and control samples. Control sample has well-defined monomer, dimer, and trimer regions that are flattened after aging, as indicated by the boxes. Panel (b) shows the distribution of the number of carbon atoms in assigned compounds that flattens in the aged sample. Panel (c) shows the double bond equivalent (DBE) as a function of the number of carbon atoms per assigned molecule for both aged and control samples. Aged sample compounds have a higher DBE compared to control samples.

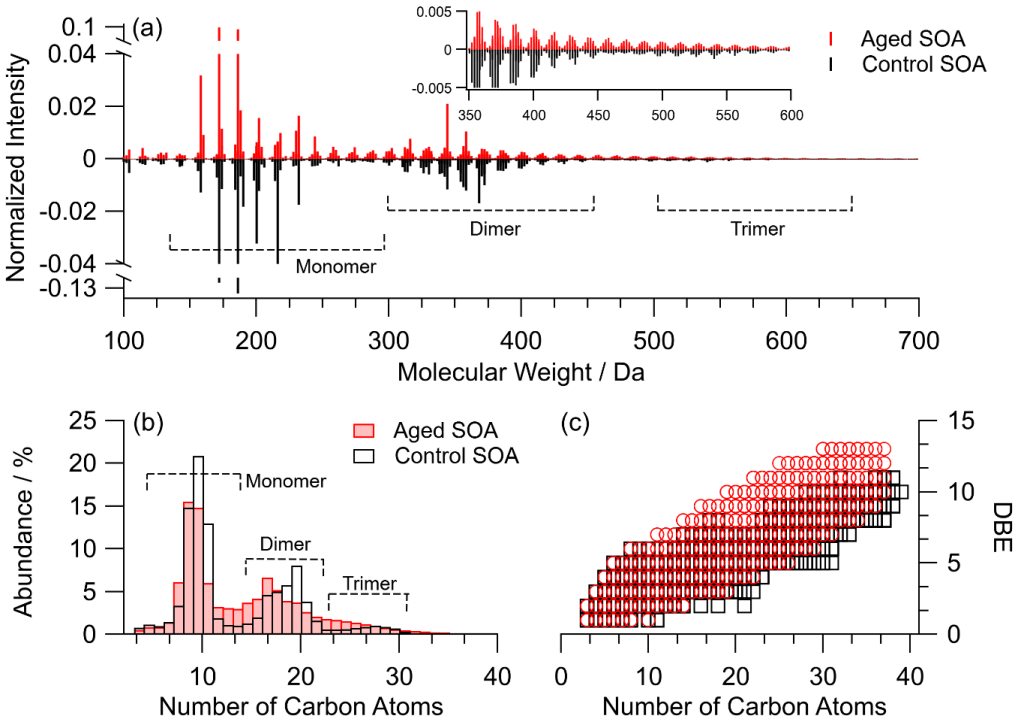

Figure S7: High resolution mass spectrometry (HRMS) analysis of α-pinene ozonolysis SOA produced in the flow tube and changes in chemical composition due to aging. Panel (a) shows mass spectra of the aged and control samples. Control sample has well-defined monomer, dimer, and trimer regions that are flattened after aging, as indicated by the boxes. Panel (b) shows the distribution of the number of carbon atoms in assigned compounds that flattened in the aged samples. Panel (c) shows the double bond equivalent (DBE) as a function of the number of carbon atoms per assigned molecule for both aged and control samples. Aged SOA compounds have a higher DBE compared to control samples.

Prediction of SOA Viscosity Based on HRMS Data

Viscosity as a function of RH was predicted using the method described by DeRieux et al. (2018)[25]. This method involves predicting the glass transition temperature from molecular composition. Following this approach, the glass transition temperature $T_{g,i}$ for a single compound i is given by:

$$T_{g,i} = (n_C^0 + \ln(n_C))b_C + \ln(n_H)b_H + \ln(n_C)\ln(n_H)\,b_{CH} + \ln(n_O)\,b_O + \ln(n_C)\ln(n_O)\,b_{CO}, \quad (S1)$$

where n_C, n_H, and n_O are the number of carbon, hydrogen, and oxygen atoms in compound i, respectively. Values of coefficients are 12.13, 10.95, -41.82, 21.61, 118.96, and -24.38 for n_C^0, b_C, b_H, b_{CH}, b_O, and b_{CO}, respectively.

The T_g of the SOA under dry conditions ($T_{g,org}$) was estimated using the Gordon-Taylor equation (eq. S2), and assuming a Gordon Taylor constant of 1 for each organic component within the SOA[26]:

$$T_{g,org} = \sum_i w_i T_{g,i}\ , \quad (S2)$$

where w_i is the mass fraction of an organic compound i in the mixture[26]. For all HRMS-based viscosity predictions, w_i was calculated using the peak abundances from the HRMS data (I_i) while correcting for the overionization of compounds with higher unsaturation (represented by the $(H{:}C)_i$ ratio) and molecular weight (M_i) using the method developed by Nguyen et al. (2013) (eq. S3)[27]. Note that we assumed the effective limit of detection to be zero. This is a reasonable approximation, as previous work has demonstrated that limit of detection decreased quickly at higher adjusted mass[27]. In our experiments, over 90% of detected compounds have an adjusted mass larger than 250 Da, resulting in a small limit of detection (LOD). For comparison, the T_g of the SOA under dry conditions, not correcting for overionization of compounds, ($T_{g,org,uncorr}$) was also calculated using eq. S2, but setting $w_i = I_i$, and is shown in Table S3.

$$w_i = \frac{I_i}{adjusted\ mass} = \frac{I_i}{(H{:}C)_i \times M_i}. \quad (S3)$$

The $T_{g,org}$ was then used to calculate the corresponding viscosity using modified forms of the Vogel-Tammann-Fulcher (VTF) equation[25]:

$$\eta(RH,T) = \eta_\infty e^{\frac{T_0(RH)D_{\text{frag}}}{T-T_0(RH)}}, \qquad (S4)$$

where η_∞ is the viscosity at infinite temperature (10^{-5} Pa s)[28,29], D_{frag} is the fragility parameter, and $T_0(RH)$ is the RH-dependent Vogel temperature. Rearranging eq. S4 and solving for $T_0(RH)$ yields:

$$T_0(RH) = \frac{\ln\left(\frac{\eta(RH,292\text{ K})}{\eta_\infty}\right) * (292\text{ K})}{D_{\text{frag}} + \ln\left(\frac{\eta(RH,292\text{ K})}{\eta_\infty}\right)}. \quad (S5)$$

The fragility parameter describes the deviation from an ideal Arrhenius behavior of the temperature dependence of viscosity[25]. Here, we assumed a value of $D_{\text{frag}} = 10$ based on DeRieux et al.[25] and Shiraiwa et al.[30] who showed a correlation between D_{frag} and molar mass, with the fragility reaching a lower limit of 10.3 at higher molar masses, starting at ~200 g mol^{-1} (overlapping with the average molar mass of SOA studied here). We further assumed the fragility parameter to be independent of RH, as done previously[25,30–32]. Petters and Kasparoglu (2020)[33] suggested a fragility parameter of 7 for α-pinene SOA, which is close to our assumed value (we further explore the sensitivity of predictions to D_{frag} below).

Modifying the VTF equation (eq. S4 and S5) by assuming the viscosity at infinite temperature to be 10^{-5} Pa s, and the viscosity at the glass transition temperature to be 10^{12} Pa s[29] yields:

$$\log(\eta) = -5 + 0.434\frac{T_0 D_{frag}}{T - T_0}, \quad (S6)$$

$$T_0(RH) = \frac{39.17 T_{g,org}}{D_{frag} + 39.17}. \quad (S7)$$

Here, η is the viscosity of the organic mixture, D_{frag} is the fragility constant (assumed to have a value of 10; see above), and T is the temperature at which the viscosity measurements were performed (292 K). To convert from $T_{g,org}$ to η, we assumed a fragility parameter of 10 for both the aged and control samples. While this is a commonly used value and corresponds to the lower limit of 10.3 at higher molar masses, values between 5-15 are also plausible.[25] Thus, it could be possible that the control and aged SOA materials have different fragilities with different fragility values. Predicting SOA viscosity using different fragility parameters (i.e., 5 for control SOA and 10 for aged SOA) would correct for the overpredicted control SOA viscosity seen here. While a fragility lower than 10 would be consistent with the suggested value of 7 for α-pinene SOA,[33] it is difficult to justify why the control sample would require a different parameter than the aged one. More information on the fragility of organic mixtures is needed to more accurately select the fragility values used to convert $T_{g,org}$ into viscosity.

Section S3: Calculations and Parameterizations for Viscosity and Mixing Times of Organic Molecules within SOA

Diffusion Coefficients and Mixing Times of Organic and Water Molecules

Viscosities (η) can be used to calculate diffusion coefficients of the organic molecules (D_{org}) within the SOA, using the (classical) Stokes-Einstein (SE) relation[34]:

$$D_{\mathrm{org}}(RH,T) = \frac{kT}{6\pi\eta(RH,T)R_{\mathrm{diff}}}, (S8)$$

where k is the Boltzmann constant, T is the absolute temperature in units of Kelvin, and R_{diff} denotes the hydrodynamic radius of the diffusing organic molecule. Here, we estimated R_{diff} to be 0.44 nm and 0.42 nm for UV-aged and control SOA particles, respectively, for SOA derived from d-limonene ozonolysis[35]. These estimates are based on the average molecular weights of the SOA (270 g mol^{-1} for aged SOA; 246 g mol^{-1} for control SOA; see Table S3), an assumed material density of 1.3 g cm^{-3} [36–38], and spherical geometry for the diffusing organic molecules. Diffusion coefficients estimated using the SE equation have been found to be in reasonable agreement with measured diffusion coefficients of organic molecules if the radius of the diffusing molecules is equal or greater than the radius of the molecules making up the (organic) matrix (R_{matrix}), and if the SOA particle viscosities are between 10^{-3} to 10^{10} Pa s[39].

To calculate diffusion coefficients of water molecules, $D_{\mathrm{H_2O}}$, we used the fractional SE equation [40–44]. The classical SE equation was not used in this case, since the radius of water (0.1 nm) is less than the radius of molecules making up the organic matrix (0.44 nm and 0.42 nm for UV-aged and control SOA particles)[45]. The fractional SE is expressed as:

$$D_{\mathrm{H_2O}}(RH,T) = D_{\mathrm{o}}(T) * \left(\frac{\eta_{\mathrm{o}}(T)}{\eta(RH,T)}\right)^{\xi}. (S9)$$

Here, $D_{\mathrm{H_2O}}(RH,T)$ is the RH- and temperature-dependent diffusion coefficient of water in SOA, $D_o(T)$ is the temperature-dependent diffusion coefficient of water in pure water calculated from the SE equation (eq. S8) and assuming a value of 0.1 nm for R_{diff}, $\eta_o(T)$ is the temperature-dependent viscosity of pure water (10^{-3} Pa s at T = 293 K)[46], and ξ is the fractional exponent. The fractional exponent was calculated from eq. S10:

$$\xi = 1 - \left[A * \exp\left(-B\frac{R_{\mathrm{diff}}}{R_{\mathrm{matrix}}}\right)\right], \qquad (S10)$$

where, A is 0.73, and B is 1.79[45]. Here we assumed a radius of the diffusing molecules of R_{diff} = 0.1 nm, and R_{matrix} values of 0.44 nm and 0.42 nm for UV-aged and control SOA particles, respectively.

The diffusion coefficients of organic molecules were converted to characteristic mixing times, $\tau_{\mathrm{mix,dp,org}}$, using the following equation[47]:

$$\tau_{\mathrm{mix,dp,org}}(RH,T) = \frac{d_{\mathrm{p}}^2}{4\pi^2 D_{\mathrm{org}}(RH,T)}, \qquad (S11)$$

where d_{p} is the diameter of the SOA particles. Similarly, the diffusion coefficients of water were converted to characteristic mixing times, $\tau_{\mathrm{mix,dp,H_2O}}$, using an equation similar to S11[47]:

$$\tau_{\mathrm{mix,dp,H_2O}}(RH,T) = \frac{d_{\mathrm{p}}^2}{4\pi^2 D_{\mathrm{H_2O}}(RH,T)}. \quad (S12)$$

Mixing times denote the characteristic time required for the concentration of the diffusing molecules at the center of the aerosol particle to deviate from the thermodynamic equilibrium concentration by less than 1/*e*, assuming nonreactive gas-particle partitioning[47]. We calculated mixing times for SOA particles having a diameter of 200 nm, typical for atmospheric SOA[48–50], and corresponding to accumulation mode particles[51].

Prediction of SOA Viscosity as a Function of Relative Humidity and Temperature

The particle viscosities as a function of RH can be predicted using a mole-fraction based Arrhenius mixing rule[32,52]. This approach has previously been applied to experimentally determined viscosities for SOA derived from β-caryophyllene ozonolysis[53]. Following a similar approach, the mixing rule can be expressed as[54]:

$$\log(\eta_{\mathrm{org,wet}}) = \chi_{\mathrm{org}} \log(\eta_{\mathrm{org,dry}}) + (1-\chi_{\mathrm{org}}) \log(\eta_{\mathrm{o}}), \qquad (S13)$$

where $\eta_{\mathrm{org,wet}}$ is the viscosity of the SOA-water mixture, $\eta_{\mathrm{org,dry}}$ is the viscosity of the dry SOA material, free of water and corresponding to the experimental results at 0% RH, η_{o} is the viscosity of pure water (10^{-3} Pa s at $T = 293$ K [55]), and χ_{org} denotes the mole-fraction of organics in the SOA-water mixture. The mole-fraction of organics was calculated as:

$$\chi_{\mathrm{org}} = \frac{\frac{w_{\mathrm{org}}}{M_{\mathrm{org}}}}{\frac{w_{\mathrm{org}}}{M_{\mathrm{org}}} + \frac{1-w_{org}}{M_{\mathrm{H_2O}}}}, \qquad (S14)$$

where w_{org} is the weight fraction of the SOA, and M_{org} is the average molecular weight of the SOA determined by high resolution mass spectrometry (see Table S3).

Values of w_{org} were calculated as[56]:

$$w_{org} = \left(1 + \kappa\left(\frac{a_w}{1-a_w}\right)\right)^{-1}, \qquad (S15)$$

where a_w is the activity of water and κ is a mass-based hygroscopicity parameter of the SOA material[57]. Upon fitting eq. S13 to the RH-dependent viscosity data, κ values were determined to be 0.025 for both aged and control d-limonene SOA (Fig. S8). These κ values are solely used for the parameterization of viscosity and not to derive physical meaning from them. Parameterized viscosity as a function of RH for aged and control d-limonene SOA produced in an environmental chamber are shown in Fig. S8a,b.

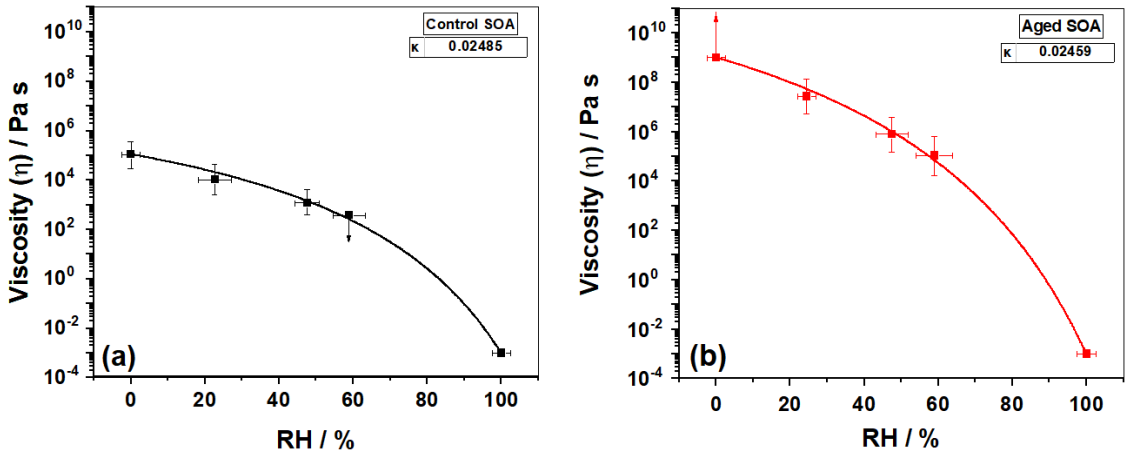

Figure S8: Parametrization of the dependence of viscosity on water activity for (a) control, and (b) aged SOA derived from d-limonene ozonolysis.

In order to extrapolate the RH-dependent, room-temperature viscosity values $\eta(RH, 292\ \mathrm{K})$ to other temperatures found in the troposphere $\eta(RH, T)$, we used the VTF equation (eq. S4)[25].

Global Distributions of Viscosity and Mixing Times of Organic and Water Molecules within SOA Using the EMAC Model

We combined our parameterization for viscosity and mixing times with average RH and temperature fields from a global climate chemistry model (European Center Hamburg Model/Modular Earth Submodel System Atmospheric Chemistry Model, EMAC) for the years 2005–2009 [58], to calculate the zonal, annual mean values of viscosity and mixing times of organic (Fig. 5, 6) and water molecules (Fig. S9) within our SOA.

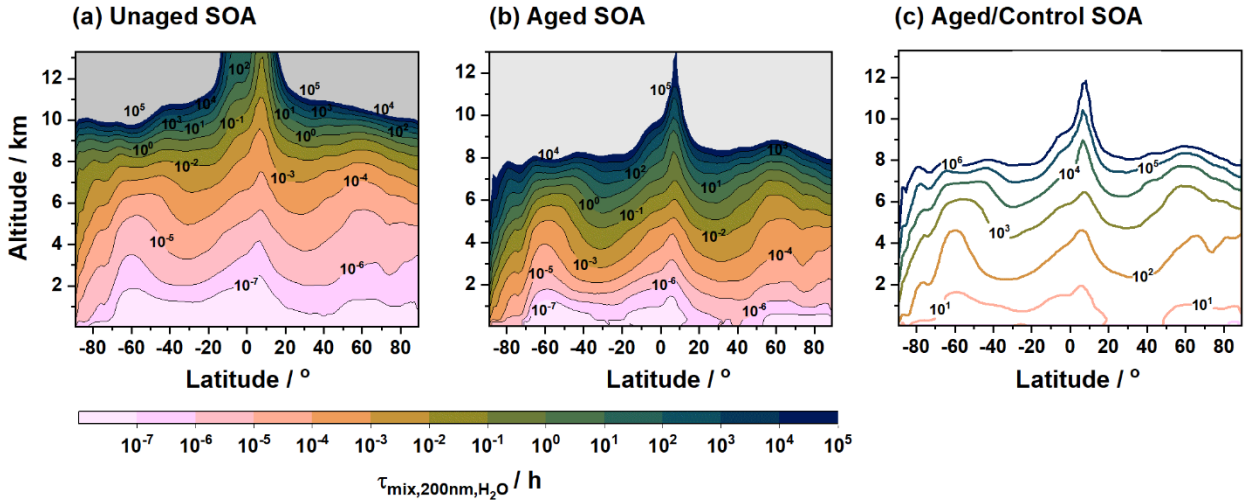

Figure S9: Zonally-averaged mixing times of water molecules within 200 nm SOA. A comparison of the effect of aging by UV-radiation on the zonally-averaged mixing times of water molecules within 200 nm SOA. Panels (a) and (b) represent spatial distribution of mixing times of water molecules for control and aged d-limonene SOA, respectively. Panel (c) represents the ratio of mixing times of water molecules of aged and control d-limonene SOA. Grey shaded areas indicate that mixing times of water molecules were not-determined. Data shown correspond to SOA produced in an environmental chamber by ozonolysis.

Section S4: SOA UV-Aging Methods

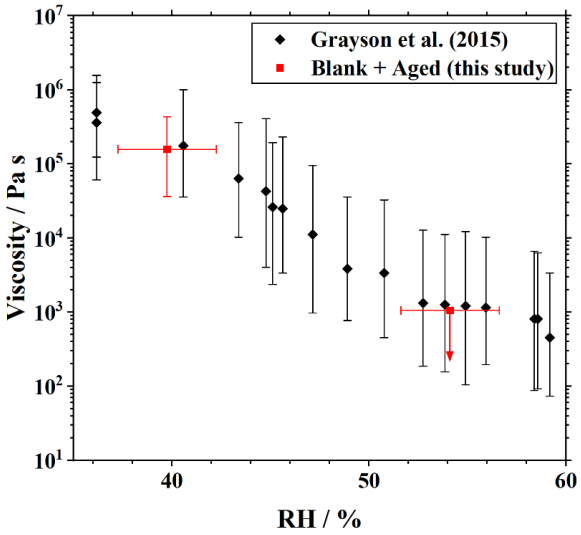

Figure S10: Control Experiments show that aging of hydrophobic coatings on glass slides by UVexposure does not affect the viscosity measurements. This was done by nebulizing sucrose-water particles onto a hydrophobic glass slide coated with Fluoropel 800 (CYTONIX) after the glass slide had been aged by UV-radiation (for 12 days). After nebulization, the viscosity values of sucrose-water particles were determined and compared to that reported in Grayson et al. (2015)[59]. COMSOL simulation parameters used were those reported by Grayson et al. (2015)[59].

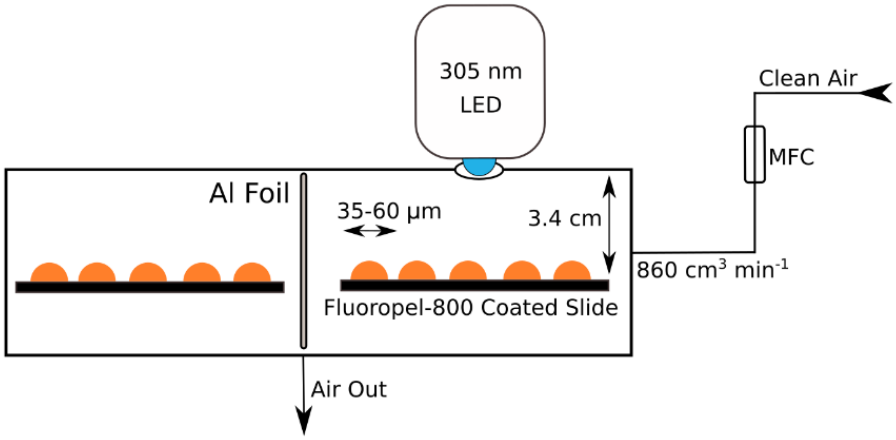

Figure S11: The chamber used to irradiate SOA substrates. SOA substrates are placed in the chamber, 3.4 cm below a 305 nm LED. Control samples are shielded from the UV radiation using a sheet of high purity aluminum foil. Clean air flows into the chamber using a mass flow controller (MFC) at a flow rate of 860 cm^3 min^{-1}. Both aged and control samples are exposed to the same amount of air flow during the aging experiment.

Spectral Flux Density in Los Angeles

We used the following parameters from the Quick TUV calculator[60,61]:

- Latitude/Longitude: 34°/-118°
- Date and Time: June 20, 2017 – data from each hour in the day were acquired and averaged to obtain a ***24-hour average*** spectral flux density.
- Overhead Ozone: 300 du
- Surface Albedo: 0.1
- Ground Altitude: 0 km
- Measured Altitude: 0 km
- Clouds Optical Depth/Base/Top: 0.00/4.00/5.00
- Aerosols Optical Depth/S-S Albedo/Alpha: 0.235/0.990/1.000
- Sunlight Direct Beam/Diffuse Down/Diffuse Up: 1.0/1.0/1.0
- 4 streams transfer model

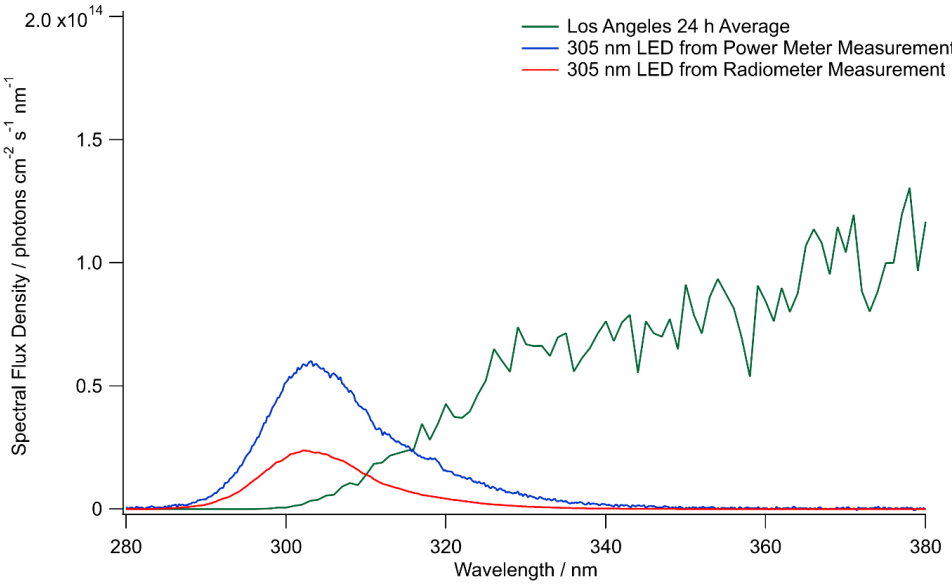

Figure S12: Spectral flux density of the M300L4 305 nm LED and the 24-h averaged Los Angeles conditions (including day and night). Los Angeles spectral flux densities were obtained using the TUV model[61]. The radiometer measurement in red is more accurate; the power meter measurement is less accurate but included because it was used in previous work[62] as a metric for the UV LED light intensity. If integrated over the 290-330 nm range, where we can expect reasonable photochemical activity, the flux from the UV-LED source is of the same order of magnitude as the solar flux. It should be pointed out that the UV-LED photons are more energetic than solar photons, and have a very different spectrum, making the exact comparison difficult.

Scaling Experimental Aging Time to Atmospheric Exposure

To estimate the UV-exposure time of SOA under atmospheric conditions, we assumed that the photodegradation rate J scales in proportion to the convolution of spectral flux $F(\lambda)$, quantum yield $\phi(\lambda)$, and absorption cross section $\sigma(\lambda)$

$$J = \int F(\lambda)\phi(\lambda)\sigma(\lambda)d\lambda. \quad (S16)$$

The absorption cross section and quantum yield of many of these molecules become small at longer wavelengths[51,63,64]. Thus, it is reasonable to limit the integration to the narrow range of the LED emission assuming that not much photodegradation occurs at longer wavelengths. For a narrow integration range, the scaling of photodegradation rates for two different light sources can be approximated as the ratio of integrated spectral flux densities

$$scaling\ factor = \frac{\int F(\lambda)_{LED} d\lambda}{\int F(\lambda)_{atmosphere} d\lambda}. \quad (S17)$$

Using these equations, the spectral flux densities of the 305 nm LED and the 24-h average Los Angeles spectrum (at sea level) were integrated from 290-330 nm. The 305 nm LED has a spectral flux of 1.0×10^{15} photons cm^{-2} s^{-1} using the power meter flux measurement. The more accurate radiometer flux measurement was 4.1×10^{14} photons cm^{-2} s^{-1}. The 24-h Los Angeles average spectrum has an average J_{NO2} value of 4.05×10^{-3} s^{-1} and spectral flux of 8.7×10^{14} photons cm^{-2} s^{-1}. Our calculated experimental scaling factor of 0.47 and 1.2 (for radiometer and power meter measurements, respectively) was used to convert experimental exposure times of 12 days into 6-14 days of time spent in the Los Angeles atmosphere.

Section S5: Phase Behavior of the SOA particles

To determine the phase behavior of the SOA studied for poke-flow experiments, particles were subjected to RH values ranging from 0% to ~100%. The particles were monitored by optical microscopy coupled with a CCD camera. The results (Fig. S13) show that the SOA particles were one homogeneous phase across the RH range for our poke-flow experiments (0% to 60%).

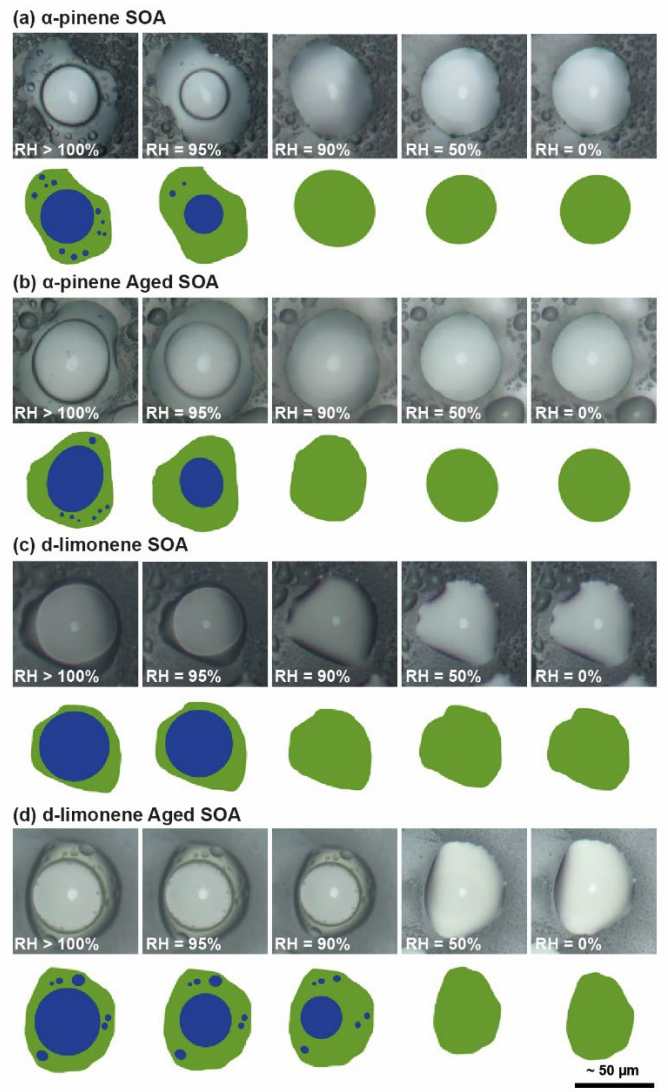

Figure S13: Optical images and illustrations of aged and unaged particles taken while decreasing relative humidity. The green color represents an organic-rich phase and the blue color represents an aqueous-rich phase. The diameter of the dry particles was ~50 µm. Panel (a) shows phase behavior for control SOA derived from α-pinene ozonolysis while panel (b) shows the phase behavior after UV-aging for the same SOA type. Panel (c) shows phase behavior for control SOA derived from d-limonene ozonolysis while panel (d) shows the phase behavior for the same SOA type after UV-aging.

References

1. Demond, A. H. & Lindner, A. S. Estimation of Interfacial Tension between Organic Liquids and Water. *Environmental Science and Technology* **27**, 2318–2331 (1993).

2. Gray Bé, A. *et al.* Cloud Activation Potentials for Atmospheric α-Pinene and β-Caryophyllene Ozonolysis Products. *ACS Central Science* **3**, 715–725 (2017).

3. Hritz, A. D., Raymond, T. M. & Dutcher, D. D. A method for the direct measurement of surface tension of collected atmospherically relevant aerosol particles using atomic force microscopy. *Atmospheric Chemistry and Physics* **16**, 9761–9769 (2016).

4. Gorkowski, K., Donahue, N. M. & Sullivan, R. C. Aerosol Optical Tweezers Constrain the Morphology Evolution of Liquid-Liquid Phase-Separated Atmospheric Particles. *Chem* **6**, 204–220 (2020).

5. Churaev, N. V, Sobolev, V. D. & Somov, A. N. Slippage of liquids over lyophobic solid surfaces. *Journal of Colloid And Interface Science* **97**, 574–581 (1984).

6. Zhu, L., Attard, P. & Neto, C. Reconciling slip measurements in symmetric and asymmetric systems. *Langmuir* **28**, 7768–7774 (2012).

7. Baudry, J., Charlaix, E., Tonck, A. & Mazuyer, D. Experimental evidence for a large slip effect at a nonwetting fluid-solid interface. *Langmuir* **17**, 5232–5236 (2001).

8. Joseph, P. & Tabeling, P. Direct measurement of the apparent slip length. *Physical Review E - Statistical, Nonlinear, and Soft Matter Physics* **71**, 1–4 (2005).

9. Vinogradova, O. I., Koynov, K., Best, A. & Feuillebois, F. Direct measurements of hydrophobic slippage using double-focus fluorescence cross-correlation. *Physical Review Letters* **102**, 1–4 (2009).

10. Tretheway, D. C. & Meinhart, C. D. Apparent fluid slip at hydrophobic microchannel walls. *Physics of Fluids* **14**, (2002).

11. McBride, S. P. & Law, B. M. Viscosity-dependent liquid slip at molecularly smooth hydrophobic surfaces. *Physical Review E - Statistical, Nonlinear, and Soft Matter Physics* **80**, 2–5 (2009).

12. Jing, D. & Bhushan, B. Boundary slip of superoleophilic, oleophobic, and superoleophobic surfaces immersed in deionized water, hexadecane, and ethylene glycol. *Langmuir* **29**, 14691–14700 (2013).

13. Craig, V. S. J., Neto, C. & Williams, D. R. M. Shear-Dependent boundary slip in an aqueous newtonian liquid. *Physical Review Letters* **87**, 54504-1-54504–4 (2001).

14. Cottin-Bizonne, C. *et al.* Nanorheology: An investigation of the boundary condition at hydrophobic and hydrophilic interfaces. *European Physical Journal E* **9**, 47–53 (2002).

15. Cottin-Bizonne, C., Cross, B., Steinberger, A. & Charlaix, E. Boundary slip on smooth hydrophobic surfaces: Intrinsic effects and possible artifacts. *Physical Review Letters* **94**, 1–4 (2005).

16. Cho, J. H. J., Law, B. M. & Rieutord, F. Dipole-dependent slip of Newtonian liquids at smooth solid hydrophobic surfaces. *Physical Review Letters* **92**, 1–4 (2004).

17. Bhushan, B., Wang, Y. & Maali, A. Boundary slip study on hydrophilic, hydrophobic, and superhydrophobic surfaces with dynamic atomic force microscopy. *Langmuir* **25**, 8117–8121 (2009).

18. Chesna, J. W. *et al.* Aerial wetting contact angle measurement using confocal microscopy. *Measurement Science and Technology* **27**, (2016).

19. Petters, S. S., Kreidenweis, S. M., Grieshop, A. P., Ziemann, P. J. & Petters, M. D. Temperature- and Humidity-Dependent Phase States of Secondary Organic Aerosols. *Geophysical Research Letters* **46**, 1005–1013 (2019).

20. Hinks, M. L. *et al.* Effect of viscosity on photodegradation rates in complex secondary organic aerosol materials. *Physical Chemistry Chemical Physics* **18**, 8785–8793 (2016).

21. Ullmann, D. A. *et al.* Viscosities, diffusion coefficients, and mixing times of intrinsic fluorescent organic molecules in brown limonene secondary organic aerosol and tests of the Stokes-Einstein equation. *Atmospheric Chemistry and Physics* **19**, 1491–1503 (2019).

22. Grayson, J. W. *et al.* Effect of varying experimental conditions on the viscosity of α-pinene derived secondary organic material. *Atmospheric Chemistry and Physics* **16**, 6027–6040 (2016).

23. Galeazzo, T. *et al.* Estimation of secondary organic aerosol viscosity from explicit modeling of gas-phase oxidation of isoprene and α-pinene. *Atmospheric Chemistry and Physics* **21**, 10199–10213 (2021).

24. Zhang, Y. *et al.* Changing shapes and implied viscosities of suspended submicron particles. *Atmospheric Chemistry and Physics* **15**, 7819–7829 (2015).

25. DeRieux, W. S. W. *et al.* Predicting the glass transition temperature and viscosity of secondary organic material using molecular composition. *Atmospheric Chemistry and Physics* **18**, 6331–6351 (2018).

26. Dette, H. P., Qi, M., Schröder, D. C., Godt, A. & Koop, T. Glass-forming properties of 3-methylbutane-1,2,3-tricarboxylic acid and its mixtures with water and pinonic acid. *Journal of Physical Chemistry A* **118**, 7024–7033 (2014).

27. Nguyen, T. B., Nizkorodov, S. A., Laskin, A. & Laskin, J. An approach toward quantification of organic compounds in complex environmental samples using high-resolution electrospray ionization mass spectrometry. *Analytical Methods* **5**, 72–80 (2013).

28. Angell, C. A. Relaxation in liquids, polymers and plastic crystals - strong/fragile patterns and problems. *Journal of Non-Crystalline Solids* **131–133**, 13–31 (1991).

29. Angell, C. A. Liquid fragility and the glass transition in water and aqueous solutions. *Chemical Reviews* **102**, 2627–2650 (2002).

30. Shiraiwa, M. *et al.* Global distribution of particle phase state in atmospheric secondary organic aerosols. *Nature Communications* **8**, 1–7 (2017).

31. Marsh, A. *et al.* Amorphous phase state diagrams and viscosity of ternary aqueous organic/organic and inorganic/organic mixtures. *Physical Chemistry Chemical Physics* **20**, 15086–15097 (2018).

32. Rothfuss, N. E. & Petters, M. D. Characterization of the temperature and humidity-dependent phase diagram of amorphous nanoscale organic aerosols. *Physical Chemistry Chemical Physics* **19**, 6532–6545 (2017).

33. Petters, M. & Kasparoglu, S. Predicting the influence of particle size on the glass transition temperature and viscosity of secondary organic material. *Scientific Reports 2020 10:1* **10**, 1–10 (2020).

34. Einstein, A. On the motion of small particles suspended in liquids at rest required by the molecular-kinetic theory of heat. *Annalen der physik* **17**, 549–560 (1905).

35. Renbaum-Wolff, L. *et al.* Viscosity of a-pinene secondary organic material and implications for particle growth and reactivity. *Proc Natl Acad Sci U S A* **110**, 8014–8019 (2013).

36. Chen, X. & Hopke, P. K. Secondary organic aerosol from α-pinene ozonolysis in dynamic chamber system. *Indoor Air* **19**, 335–345 (2009).

37. Ng, N. L., Keywood, M. D., Bahreini, R., Lee, A. & Goldstein, A. H. Contribution of First- versus Secondary Organic Aerosols Formed Hydrocarbons. *Environmental Science & Technology* **40**, 2283–2297 (2006).

38. Saathoff, H. *et al.* Temperature dependence of yields of secondary organic aerosols from the ozonolysis of α-pinene and limonene. *Atmospheric Chemistry and Physics* **9**, 1551–1577 (2009).

39. Evoy, E. *et al.* Predictions of diffusion rates of large organic molecules in secondary organic aerosols using the Stokes-Einstein and fractional Stokes-Einstein relations. *Atmospheric Chemistry and Physics* **19**, 10073–10085 (2019).

40. Bastelberger, S., Krieger, U. K., Luo, B. & Peter, T. Diffusivity measurements of volatile organics in levitated viscous aerosol particles. *Atmospheric Chemistry and Physics* **17**, 8453–8471 (2017).

41. Price, H. C. *et al.* Water diffusion in atmospherically relevant α-pinene secondary organic material. *Chemical Science* **6**, 4876–4883 (2015).

42. Davies, J. F. & Wilson, K. R. Raman Spectroscopy of Isotopic Water Diffusion in Ultraviscous, Glassy, and Gel States in Aerosol by Use of Optical Tweezers. *Analytical Chemistry* **88**, 2361–2366 (2016).

43. Price, H. C., Mattsson, J. & Murray, B. J. Sucrose diffusion in aqueous solution. *Physical Chemistry Chemical Physics* **18**, 19207–19216 (2016).

44. Marshall, F. H. *et al.* Diffusion and reactivity in ultraviscous aerosol and the correlation with particle viscosity. *Chemical Science* **7**, 1298–1308 (2016).

45. Evoy, E., Kamal, S., Patey, G. N., Martin, S. T. & Bertram, A. K. Unified Description of Diffusion Coefficients from Small to Large Molecules in Organic-Water Mixtures. *Journal of Physical Chemistry A* **124**, 2301–2308 (2020).

46. Crittenden, J., Trussell, R., Hand, D., Howe, K. & Tchobanoglous, G. *MWH's Water Treatment: Principles and Design*. (John Wiley & Sons, 2012).

47. Seinfeld, J. H. & Pandis, S. N. *Atmospheric Chemistry and Physics*. (Wiley, 2006).

48. Martin, S. T. *et al.* An overview of the Amazonian Aerosol Characterization Experiment 2008 (AMAZE-08). *Atmospheric Chemistry and Physics* **10**, 11415–11438 (2010).

49. Pöschl, U. *et al.* Rainforest Aerosols as Biogenic Nuclei of Clouds and Precipitation in the Amazon. *Science (1979)* **329**, 1513–1516 (2010).

50. Riipinen, I. *et al.* Organic condensation: A vital link connecting aerosol formation to cloud condensation nuclei (CCN) concentrations. *Atmospheric Chemistry and Physics* **11**, 3865–3878 (2011).

51. Finlayson-Pitts, B. J. & Pitts, J. N. *Chemistry of the Upper and Lower Atmosphere: Theory, Experiments, and Applications*. (Academic Press, 2000).

52. Centeno, G., Sánchez-Reyna, G., Ancheyta, J., Muñoz, J. A. D. & Cardona, N. Testing various mixing rules for calculation of viscosity of petroleum blends. *Fuel* **90**, 3561–3570 (2011).

53. Maclean, A. M. *et al.* Humidity-Dependent Viscosity of Secondary Organic Aerosol from Ozonolysis of β-Caryophyllene: Measurements, Predictions, and Implications. *ACS Earth and Space Chemistry* **5**, 305–318 (2021).

54. Zhmud, B. Viscosity Blending Equations. *Lube Magazine* 2–5 (2014).

55. Crittenden, J. C., Trussell, R. R., Hand, D. W., Howe, K. J. & Tchobanoglous, G. *MWH ' s Water Treatment - Principles and Design*. (John Wiley & Sons, Inc., Hoboken, New Jersey, 2012).

56. Rothfuss, N. E. & Petters, M. D. Characterization of the temperature and humidity-dependent phase diagram of amorphous nanoscale organic aerosols. *Physical Chemistry Chemical Physics* **19**, 6532–6545 (2017).

57. Petters, M. D. & Kreidenweis, S. M. A single parameter representation of hygroscopic growth and cloud condensation nucleus activity. *Atmospheric Chemistry and Physics* 1961–1971 (2007) doi:10.5194/acp-13-1081-2013.

58. Maclean, A. M. *et al.* Global Distribution of the Phase State and Mixing Times within Secondary Organic Aerosol Particles in the Troposphere Based on Room-Temperature Viscosity Measurements. *ACS Earth and Space Chemistry* **5**, 3458–3473 (2021).

59. Grayson, J. W., Song, M., Sellier, M. & Bertram, A. K. Validation of the poke-flow technique combined with simulations of fluid flow for determining viscosities in samples with small volumes and high viscosities. *Atmospheric Measurement Techniques* **8**, 2463–2472 (2015).

60. Madronich, S. & Flocke, S. The role of solar radiation in atmospheric chemistry. *Handbook of Environmental Chemistry (P. Boule, ed.)* 1–26 (1998).

61. Madronich, S. Tropospheric ultraviolet and visible (TUV) radiation model. https://www2.acom.ucar.edu/modeling/tropospheric-ultraviolet-and-visible-tuv-radiation-model.

62. Baboomian, V. J., Gu, Y. & Nizkorodov, S. A. Photodegradation of Secondary Organic Aerosols by Long-Term Exposure to Solar Actinic Radiation. *ACS Earth and Space Chemistry* **4**, 1078–1089 (2020).

63. Malecha, K. T., Cai, Z. & Nizkorodov, S. A. Photodegradation of Secondary Organic Aerosol Material Quantified with a Quartz Crystal Microbalance. *Environmental Science and Technology Letters* **5**, 366–371 (2018).

64. Fagnoni, M. Modern Molecular Photochemistry of Organic Molecules. By Nicholas J. Turro, V. Ramamurthy and Juan C. Scaiano. *Angewandte Chemie International Edition* **49**, 6709–6710 (2010).